Probing Lattice Dynamics in Two-Dimensional Inorganic Pseudohalide Perovskites with Ultrafast Infrared Spectroscopy

Xiangyu Xing[§,1], Jiayi Li [§,1], John P. Breen[§,1], Jun Nishida[3], Hemamala I. Karunadasa[#,1,2], and Michael D. Fayer*[,1]

1. Department of Chemistry, Stanford University, Stanford, CA 94305 USA
2. Stanford Institute for Materials and Energy Sciences, SLAC National Accelerator Laboratory, Menlo Park, California 94025, USA
3. Center for Mesoscopic Sciences, Institute for Molecular Science, Okazaki, Aichi 444-8585, Japan

[#]Email: hemamala@stanford.edu, Phone: 650 723-0288
*Email: fayer@stanford.edu, Phone: 650 723-4446

Supporting Information

1. Profilometry Measurement of the $Cs_2Pb(SCN)_2Br_2$ (Br^-) Film

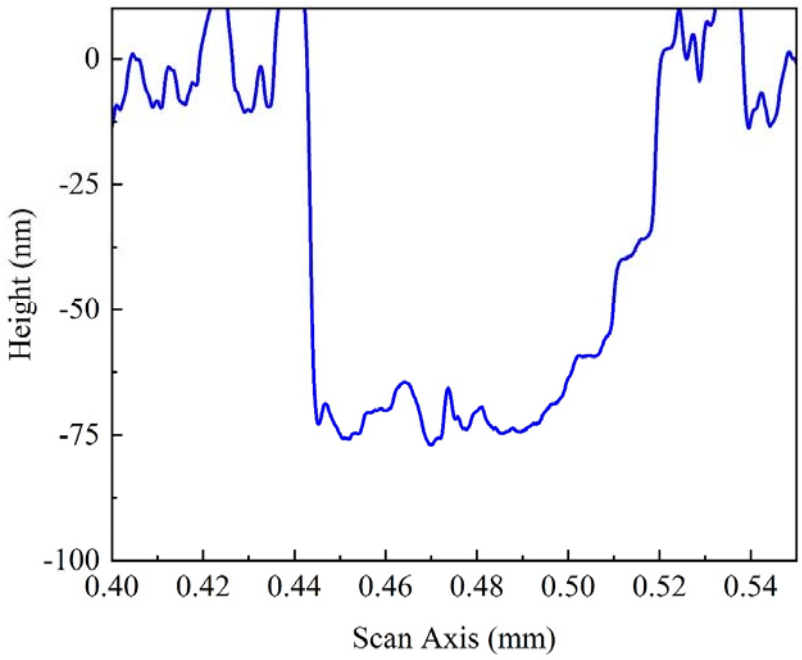

Figure S1. Surface profilometry. The scans were done across a cut on the sample, and the film thickness was determined to be ~70 nm.

2. Single-Crystal X-ray Diffraction (SC-XRD)

Single crystals of $Cs_2Pb(SCN)_2Br_2$ were formed following the reported method in a nitrogen glovebox.[1] The crystals were kept in a nitrogen atmosphere before the measurements, coated with Paratone-N® oil, and then mounted on a Kapton® loop. The data were collected using a Bruker D8 diffractometer equipped with a Photon II CMOS detector at the Stanford Nano Shared Facilities (17.445 keV Mo-Kα radiation, λ = 0.71073 Å). During the course of measurements at

Table S1 Crystallographic data for $Cs_2Pb(SCN)_2Br_2$

Compound	$Cs_2Pb(SCN)_2Br_2$
Empirical Formula	$Cs_2PbS_2C_2N_2Br_2$
Formula Weight, g/mol	748.99
Temperature, K	296.15
Crystal System	Orthorhombic
Space group	*Pmmn*
a, Å	17.8798(8)
b, Å	5.9709(3)
c, Å	6.0199(3)
α, °	90
β, °	90
γ, °	90
Volume, Å^3	642.68(5)
Z	2
Density (calculated), g/cm3	3.870
Absorption coefficient, mm^{-1}	25.203
F(000)	640
Crystal size, mm^3	0.04 × 0.04 × 0.015
2θ range, °	3.384 to 33.152
Index ranges	$-24 \le h \le 27$ $-9 \le k \le 9$ $-9 \le l \le 9$
Reflections collected/unique	11974/4781
Completeness to θ_{max}	0.999
Data/restraints/parameters	1352/0/37
Goodness-of-fit on F^2	1.087
Final *R* indices [$I > 2\sigma(I)$][a]	$R_1 = 0.0218$ w$R_2 = 0.0402$
R indices (all data)[a]	$R_1 = 0.0275$ w$R_2 = 0.0420$
Largest diff. peak and hole, e/Å^{-3}	0.633, –1.226

[a] $R_1 = \Sigma||F_o| - |F_c||/\Sigma|F_o|$, w$R_2 = [\Sigma w(F_o^2 - F_c^2)^2/\Sigma(F_o^2)^2]^{1/2}$

room temperature, a flow of N_2 enveloped the crystal and it didn't show signs of degradation. The unit-cell parameters were refined against all data. Frames were collected using ω and φ scans, integrated and corrected for Lorentz and polarization effects using SAINT 8.34a, and then corrected for absorption effects using SADABS V2014.[2] Space-group assignments were based on systematic absences, *E*-statistics, agreement factors for equivalent reflections, and successful refinement of the structures. The structures were solved by direct methods and refined against all data using the SHELXL-2014[3] software package as implemented in Olex2.[4]

3. Powder X-ray Diffraction of $Cs_2Pb(SCN)_2X_2$ films

The thin films for PXRD measurements were fabricated using the same methods as the ones used for 2D-IR but with higher precursor concentrations to increase the diffraction intensity. The I^- film was coated with a layer of poly(methyl methacrylate) (PMMA) to avoid degradation during measurements. The PXRD measurements were performed under ambient conditions on a Bruker D8 Advance diffractometer equipped with a Cu anode ($K\alpha_1$ = 1.54060 Å, $K\alpha_2$ = 1.54443 Å, $K\alpha_2/K\alpha_1$ = 0.5), fixed divergence slits with a nickel filter, and an LYNXEYE detector. The simulated powder patterns were calculated using the crystallographic files (CIFs) from single-crystal X-ray experiments or downloaded from a database.

By comparing the PXRD patterns of the precursors or possible side phases, we concluded that the I^- film was phase pure (Figure S2). The PXRD peaks could be correlated to the simulated patterns of $Cs_2Pb(SCN)_2Br_2$. Assuming that $Cs_2Pb(SCN)_2I_2$ adopts the same space group and all the atoms remain at the same coordinates, we can calculate the unit-cell axes using the PXRD reflections and their corresponding Miller indices. The simulated PXRD pattern of $Cs_2Pb(SCN)_2I_2$ matches well with the experimental data of the I^- film (Figure S3).

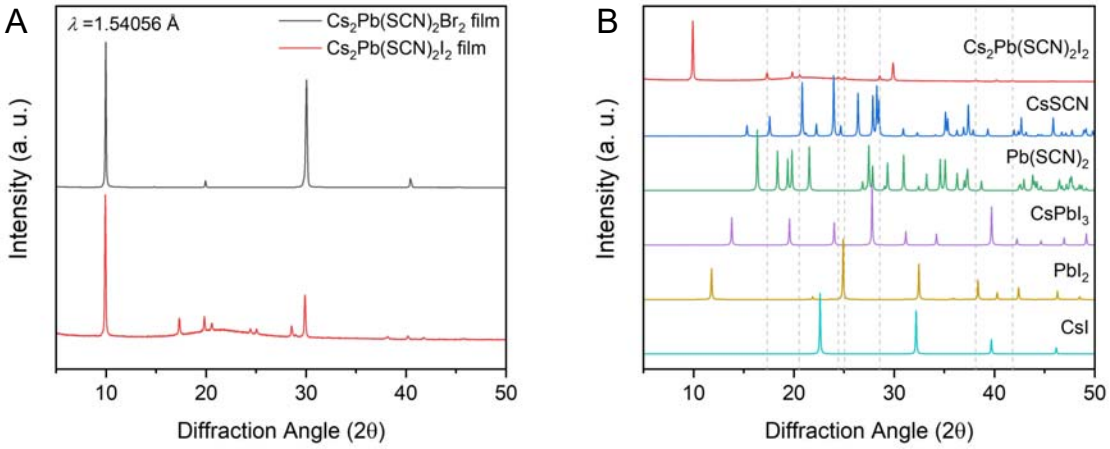

Figure S2. (A) PXRD patterns of the Br^- and I^- films. The I^- film shows less preferential orientation. (B) Comparison of the PXRD pattern of the I^- film with the PXRD patterns of possible side products or precursors.

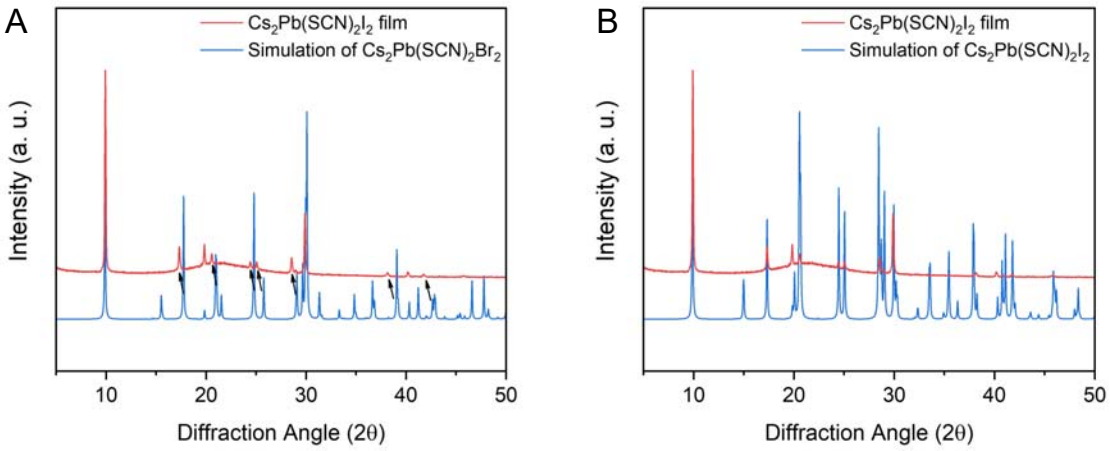

Figure S3. (A) PXRD pattern of the I^- film overlaid with the simulated PXRD pattern obtained from the room-temperature single-crystal structure of $Cs_2Pb(SCN)_2Br_2$. (B) PXRD pattern of the I^- film overlaid with the simulated PXRD pattern obtained from the calculated structure of $Cs_2Pb(SCN)_2I_2$.

4. FT-IR Spectrum of $Pb(SCN)_2$

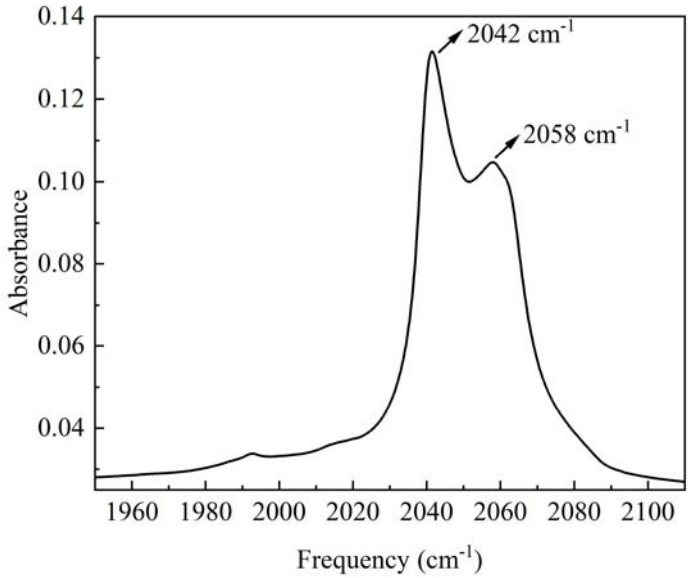

Figure S4. The FT-IR spectrum of the $Pb(SCN)_2$ film. The peaks at 2042 cm^{-1} and 2058 cm^{-1} correspond to the ^{12}CN stretch.

5. FT-IR Spectrum of Cs(SCN)

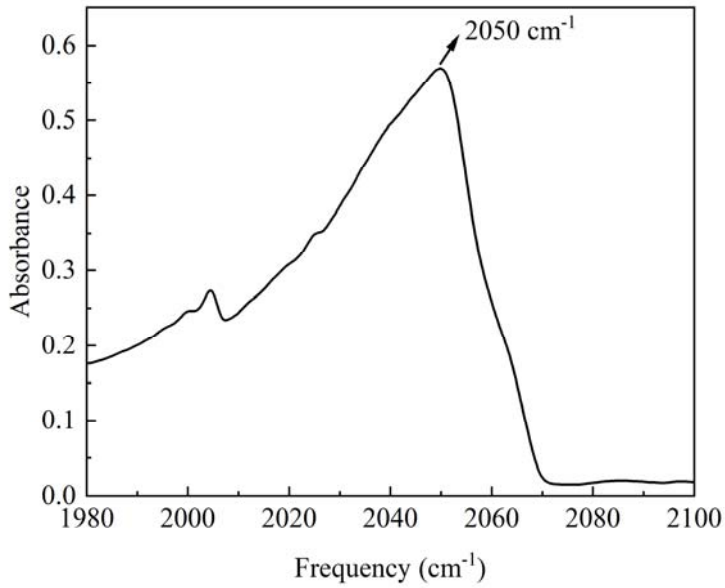

Figure S5. The FT-IR spectrum of Cs(SCN) powder. The peak corresponding to the ^{12}CN stretch is located at ~2050 cm^{-1}. The Cs(SCN) was synthesized following a reported method.[5]

6. The Small-Incidence Angle Reflection PSPP Method

As mentioned in the main text, the polarization-selective pump-probe (PSPP) experiments were performed in the small-incidence reflection geometry, using s-polarization for the probe beam. Here we will briefly explain why this geometry was used. Figure S6 shows a diagram of the geometry, along with the definition of the coordinate axes.

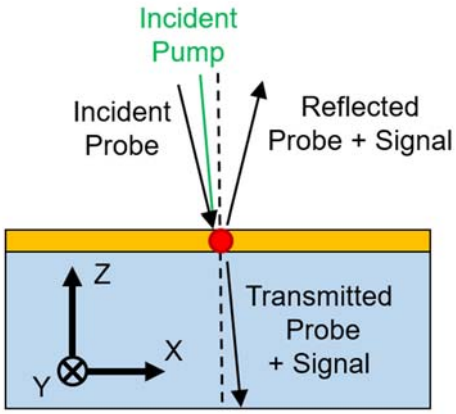

Figure S6. Schematic diagram of the small-incidence experimental geometry, along with the definition of the coordinate axes. All of the beams' propagation axes are nearly parallel to the Z-axis.

As shown previously by Nishida *et al.*[6], the reflection pump-probe signal is largest when (1) the probe beam is p-polarized, and (2) the probe incident angle is near Brewster's angle, which is typically around 54.5º. However, performing a PSPP experiment with such large incident angles adds additional theoretical complications. Briefly, the main issue is that if the incident angles are large, then the electric field components of the pump and probe beams in the Z direction (see Figure S6) are nonnegligible. These out-of-plane projections cause the observed "parallel" and "perpendicular" signals to become mixtures of the true parallel and perpendicular signals. Consequently, if the anisotropy is naively calculated from the large-incidence observed signals, the result will be significantly inaccurate. These theoretical considerations will be described in more detail in a forthcoming publication.

Therefore, for the PSPP experiments in this work, we kept the incident angles small. The probe incident angle was 18 degrees, and the pump incident angle was 2 degrees. In addition, we used s-polarization for the probe beam; this means that the probe beam had a zero electric field component in the Z direction, further reducing the out-of-plane projection issue. The pump beam was polarized at +45º, as is typical for PSPP experiments. The reflected probe beam was then resolved at ±45º to extract the parallel and perpendicular signals.

We have calculated the value of the anisotropy that would theoretically be observed as a function of the incident angle. The results are shown in Figure S7. For the case of the reflection experiment with the s-polarized probe (magenta curve), the value closely approximates the correct value (anisotropy = 0.4) for small incident angles.

Note that the disadvantage of the small-incidence reflection geometry is that the signal enhancement factor is reduced. With small incidence, the enhancement factor relative to the transmission signal is ~5 (compared to ~50 for the near-Brewster geometry[1]). However, this modest enhancement still produces significantly better signal-to-noise than the transmission experiment.

Generally, the anisotropy is written as $r(t) = 0.4C_2(t)$. Therefore, at $t = 0$, $C_2(t) = 1$, and $r(0) = 0.4$. However, implicit in this statement is that both the pump pulse and the probe pulse are normal to the sample. In practice, if the pump and probe both make a very small angle to the normal, the $r(0)$ value is very close to 0.4. In the graph below, if the pump and probe are at +8° and –8°, respectively, $r(0) = 0.401$. For angles less than plus and minus 6°, $r(0)$ is effectively 0.4. However, in the reflection geometry, the optics used to bring the pump and probe pulses into the sample make it necessary to have the probe angle relatively large so that the probe plus signal path misses the optics upon reflection. This consideration resulted in the geometry used in the pump-probe experiments. We have calculated the value of the anisotropy that would theoretically be observed at $t = 0$ as a function of incident angle for a 3D isotropic sample. The results are shown in Figure S7. For the experimental conditions used in this work, reflection experiment, s-polarized probe, $\theta_i = 18^o$, $\theta_{cross} = 16^o$ (pump 2° from normal), the value is 0.391 (compared to the pump and probe near normal value of 0.4). For the calculation of the cone angle discussed in the main text, this deviation from the theoretical value was accounted for by linearly mixing the parallel and perpendicular signals according to the following equations:

$$I_{para,mixed} = \cos\theta_{mix} I_{para} - \sin\theta_{mix} I_{perp}$$

$$I_{perp,mixed} = \sin\theta_{mix} I_{para} + \cos\theta_{mix} I_{perp}$$

The value of θ_{mix} was set to 0.432º to reproduce the initial anisotropy value of 0.391 for an isotropic sample. Then the parallel and perpendicular signals were mixed in the same way, with the same value of θ_{mix}, when doing the tilted cone angle calculation. In this way, the nonzero probe incident angle was taken into account.

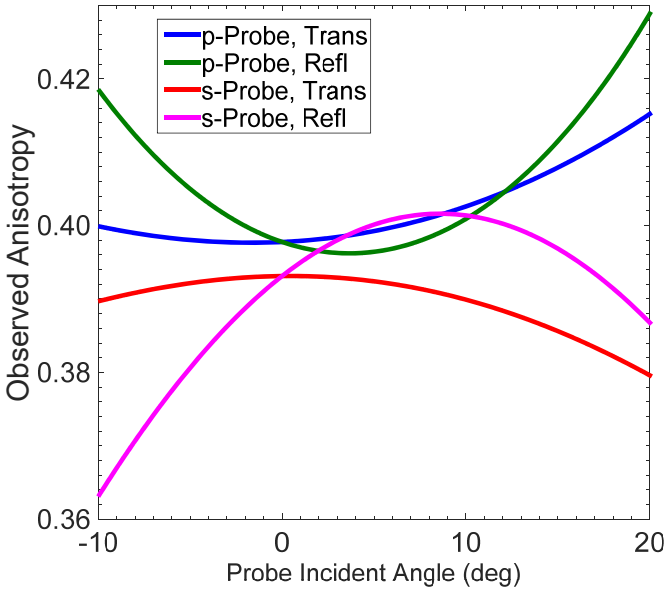

Figure S7. Calculated observed anisotropy vs. probe incident angle for a 3D isotropic sample, for both probe polarizations (p and s) and both experimental geometries, transmission and

reflection. The calculations were done with $C_2(t) = 1$ (anisotropy is 0.4 for near normal pump and probe) and a pump-probe crossing angle of 16º.

7. Population Decay of the $(MA\text{-}d_6)_2Pb(SCN)_2I_2$ Film

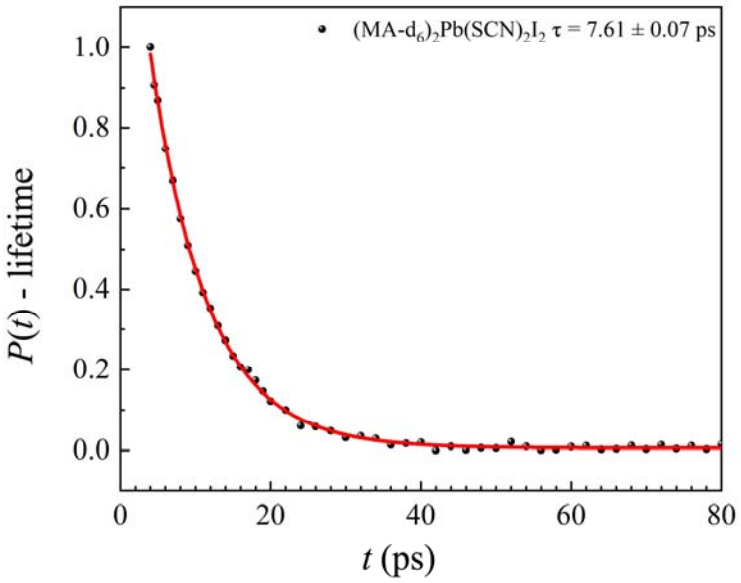

Figure S8. CN stretch vibrational population decay (lifetime) for the $(MA\text{-}d_6)_2Pb(SCN)_2I_2$ film, data (points), and single exponential fit (solid curve). The vibrational lifetime was determined to be 7.61 ± 0.07 ps.

References

1. Liao, C.-H., et al., Inorganic-Cation Pseudohalide 2D $Cs_2Pb(SCN)_2Br_2$ Perovskite Single Crystal. *Adv. Mater.* **2022**, *34*, 2104782.

2. SADABS, B. S. a., Bruker AXS Inc.: Madison, WI. **2016**.

3. Sheldrick, G. M., A Short History of SHELX. *Acta Crystallogr., Sect. A: Found. Crystallogr.* **2008**, *64* 112-122.

4. Dolomanov, O. V.; Bourhis, L. J.; Gildea, R. J.; Howard, J. A. K.; Puschmann, H., OLEX2: A Complete Structure Solution, Refinement and Analysis Program. *J. Appl. Crystallogr.* **2009**, *42*, 339-341.

5. Peng, Z.; Wei, Q.; Chen, H.; Liu, Y.; Wang, F.; Jiang, X.; Liu, W.; Zhou, W.; Ling, S.; Ning, Z., $Cs_{0.15}FA_{0.85}PbI_3/Cs_xFA_{1-x}PbI_3$ Core/Shell Heterostructure for Highly Stable and Efficient Perovskite Solar Cells. *Cell Rep. Phys. Sci.* **2020**, *1*, 100224.

6. Nishida, J.; Yan, C.; Fayer, M. D., Enhanced Nonlinear Spectroscopy for Monolayers and Thin Films in near-Brewster's Angle Reflection Pump-Probe Geometry. *J. Chem. Phys.* **2017**, *146*, 094201.